

Chapter 7

Modelling the GNSS Time Series: Different Approaches to Extract Seasonal Signals



Anna Klos, Janusz Bogusz, Machiel S. Bos and Marta Gruszczynska

Abstract Seasonal signatures observed within the Global Navigation Satellite System (GNSS) position time series are routinely modelled as annual and semi-annual periods with constant amplitudes over time. However, in this chapter, we demonstrate that these amplitudes can vary significantly over time, by as much as 3 mm at some stations. Different methods have been developed to estimate the time-varying curves. The advantages and disadvantages of those methods are presented for synthetic data, which mimic the real position time series, including their time-changeability and noise properties. For these series, we conclude that the Kalman filter and an adaptation of the Wiener Filter give the best results. As the Earth's lithosphere is seasonally loaded and unloaded, we also account for the non-tidal atmospheric, oceanic and continental hydrology loading effects, which contribute the most to the seasonal signatures. We demonstrate that a direct removal of loading effects leads to the significant change in the power of the GPS position time series, especially for frequencies between 8 and 80 cpy; if the noise model is not adapted to this new situation, this causes an underestimation of velocity uncertainty. Therefore, we recommend to use the Kalman filter or adaptive Wiener filter methods instead to remove the seasonal signal to ensure accurate estimates of the trend error.

Keywords Time series analysis · GNSS · Seasonal signals · Least-squares estimation · Modified Kalman filter · Singular spectrum analysis · Wavelet decomposition · Adaptive filters · Noise analysis

A. Klos (✉) · J. Bogusz · M. Gruszczynska
Faculty of Civil Engineering and Geodesy, Military University of Technology, Warsaw, Poland
e-mail: anna.klos@wat.edu.pl

M. S. Bos
Instituto Dom Luiz, Universidade da Beira Interior, Covilha, Portugal

© Springer Nature Switzerland AG 2020
J.-P. Montillet and M. S. Bos (eds.), *Geodetic Time Series
Analysis in Earth Sciences*, Springer Geophysics,
https://doi.org/10.1007/978-3-030-21718-1_7

7.1 Introduction

Nowadays, most of the geophysical phenomena are studied using Global Navigation Satellite System (GNSS) position time series, for which Global Positioning System (GPS) observations provide the longest observation span. Among others, the vertical land motion at tide gauges, plate motion or lithospheric deformation should be mentioned as the principal applications (Altamimi et al. 2016; King and Santamaría-Gómez 2016; Karegar et al. 2017; Graham et al. 2018; Montillet et al. 2018); for these, the horizontal and vertical velocities along with their uncertainties are employed. A secular motion is estimated from the GNSS position time series simultaneously with seasonal signatures and offsets; these constitute a so-called mathematical or deterministic model. The term ‘seasonal’ is to be understood as the annual plus semi-annual signal. Once the deterministic model is removed from the series, the residuals are examined with the optimal model of noise.

The noise content in the GNSS position time series has been already recognized to be preferably characterized, for both regional and global networks, by the white and power-law noises combination (among others, Mao et al. 1999; Williams et al. 2004; Bos et al. 2010; Santamaría-Gómez et al. 2011; Wang et al. 2012; Klos et al. 2016 should be mentioned). The noise content is most often examined with the Maximum Likelihood Estimation (MLE; see Langbein and Johnson 1997 or Langbein 2012) which provides the optimal noise parameters basing on the log-likelihood function values. The power-law behavior of the noise, observed for the low frequencies, is parametrized by spectral indices varying for position time series from -2 to 0 . A random-walk noise with a spectral index of -2 arises from the geodetic monument-specific instability or from the local multipath errors (Beavan 2005; King et al. 2012; Klos et al. 2015). Then, a flicker noise already pointed out to be preferred for the position time series has a spectral index of -1 . It is transferred into the series from large scale effects from hydrosphere or atmosphere which were mis- or un-modelled at the stage of data processing. Also, the satellite clocks, phase center or orbital errors are classified to the possible causes of flicker noise. A common influence of those effects on the regional network is referred to as Common Mode Errors (CME). CME has been already effectively modelled and removed from the position time series using a wide range of spatio-temporal filtration techniques (Dong et al. 2006; Gruszczynski et al. 2018). Finally, a white noise with spectral index of 0 , is a temporally uncorrelated type of noise; it brings no correlation within the series. A proper recognition and characterization of noise content is important, as it has a direct impact on the uncertainty of velocity: its character assumed in a wrong way, will lead to its under- or over-estimation (Williams 2003b; Williams et al. 2004; Santamaría-Gómez et al. 2011; Klos and Bogusz 2017).

Improper modelling of the noise is however not the only cause leading to overestimation of uncertainties. If any of the time series components, i.e. long-term trend, seasonal signatures or offsets, is assumed in a wrong way, this effect will be transferred to the residuals causing a change of its character (Williams 2003a; Bogusz and Klos 2016). On the contrary, once too much autocorrelation is removed from

the time series in a form of long term non-linear trend or seasonal components, one would observe an artificial improvement in a velocity uncertainty of up to 56% (Bogusz and Klos 2016). Blewitt and Lavallée (2002) were the first to demonstrate that replacing the pure velocity model with velocity combined with seasonal signals prolongs the time of the reliable velocity uncertainty estimation. This problem was discussed further by Bos et al. (2010) who showed that assuming a white and power-law noise combination leads to a decrease of the accuracy of the linear trend. This is, however, as showed recently by Klos et al. (2018d), directly related to the type of the power-law noise we add to the assumed combination.

A common practice is to remove the seasonal signals using the Least-Squares Estimation (LSE) approach, assuming the time-constancy of their parameters (Blewitt and Lavallée 2002). Annual and semi-annual signals (periods of 365.25 and 182.63 days) impacting the positions of the GNSS permanent station are broadly modelled (Blewitt et al. 2001; Collilieux et al. 2007) as these are mostly induced by geophysical sources and errors. Tides and transportation of mass within the Earth system modelled in a form of atmospheric, oceanic and hydrological effects (Tregoning et al. 2009; van Dam et al. 2012; Dill and Dobslaw 2013) influence seasonal signatures the most. Other contributors are thermal expansion of ground and monuments, or multi-path variations (King et al. 2008; Yan et al. 2009). Besides, systematic errors of numeric origin aliased into a GNSS solution (Penna and Stewart 2003) are also observed in the position time series; their contribution to seasonal signatures is sometimes as large as the loading effects. Beyond the annual and semi-annual signals, a draconitic year (Agnew and Larson 2007) with a period of 351.6 (Amiri-Simkooei 2013) days being an artefact of a GPS solution has to be also included in the GNSS time series modelling. Latest researches proved that its amplitudes are significant up to its eight harmonic (Amiri-Simkooei et al. 2017).

A direct approach to remove the impact the loadings might have on the position time series is to subtract them directly from these series. This has two effects. First, it reduces the root-mean-square value of the corrected GNSS position time series (Santamaría-Gómez and Mémin 2015). Secondly, the annual and semi-annual amplitudes change compared to those of original GNSS series. A combination of non-tidal atmospheric, ocean and continental hydrological loadings can explain as much as 40% of the observed annual signal or reduce the root-mean-square error of the GNSS position time series by 30% (Dong et al. 2002; Williams and Penna 2011); both values are valid for the vertical component. When removed separately, non-tidal ocean loading causes a peak-to-peak variation up to 5 mm (van Dam et al. 1997), the hydrological loading may explain half of the annual signal observed in the position time series (van Dam et al. 2001), while atmospheric loading causes deformations up to 20 mm (Petrov and Boy 2004). A direct subtraction of the environmental loadings was questioned by Santamaría-Gómez and Mémin (2015) who stated that this approach reduces a white noise component of the GPS position time series and has little in common with the real impact the loadings may have on the series.

Klos et al. (2018a) proved that parameters describing the seasonal signals derived from the crustal loadings are not constant over time. For this reason, the GPS-derived seasonal factors might be also time-variable and the commonly employed least-

squares approach might not provide the most reliable description. Therefore, these mis-modelled curves might produce larger residuals, implying increased noise levels. To meet the requirements of reliable modelling, several methods have been already developed by the geodetic community to fit the seasonal signatures into GNSS position time series. The Singular Spectrum Analysis (SSA) algorithm was firstly applied by Chen et al. (2013), followed by Xu and Yue (2015) and Gruszczynska et al. (2016) to deliver the time-varying signals present in the GNSS observations. The authors cross-compared the SSA-derived curves to the Kalman Filter (KF) approach; it was proved that both seasonal estimates are very close to each other. The latter was also employed by Didova et al. (2016) to estimate the time-varying trends and seasonal signals in the GNSS position time series which were then compared to the ones derived for the Gravity Recovery and Climate Experiment (GRACE) data.

Noise level present in the position time series may have a significant impact on the effectiveness and accuracy of the seasonal signatures estimated with various approaches. Klos et al. (2018b) addressed this problem; they examined the Wavelet Decomposition (WD), Chebyshev Polynomials (CP), KF and SSA approaches and stated that their effectiveness is directly related to the noise level characterizing individual time series. They also emphasized that a good approximation of seasonal signatures might be delivered only if the optimal separation between noise and seasonal curves is provided; no power transfer is observed between stochastic and deterministic part. A completely new solution to this problem was given by Klos et al. (2018c) who introduced the Adaptive Wiener Filter (AWF) to the geodetic community. This filter is based on the classical Wiener Filter (WF) and then adapted to the noise level present within individual series. To adapt this filter, the first-order autoregressive process is employed to model the time-varying curves, which are then refined by the level of noise.

In the following chapter, we present the comprehensive analysis of the seasonal signatures characterizing the GNSS position time series twofold. We start from the station-by-station modelling of the time-series-specific curves. In this approach, no attention is paid to the reason specific curve is caused by. Here, the simplest assumption of the time-constancy is cross-compared to the time-changeability of seasonal parameters. Then, we change the approach and account for different loading models proving their impact on the position time series. Also, we present the influence that different approaches have on the noise content. The entire analyses are presented for the vertical changes of the global set of GNSS stations.

7.2 Methods to Extract Seasonal Signals

In the following paragraph, we present the methodology to extract seasonal signals from the GNSS position time series. A time-constancy of parameters is being compared to their time-changeability.

7.2.1 Least-Squares Estimation

The position time series of the GNSS station can be mathematically described by fitting the following model into the time series:

$$y(t) = y_0 + v_y(t - t_0) + \sum_{i=1}^2 [a_i \sin(\omega_i(t - t_0)) + b_i \cos(\omega_i(t - t_0))] + \varepsilon(t) \quad (7.1)$$

where y_0 and v_y are initial position of each (North, East and Up) type and velocity, respectively. a_i and b_i are constants representing the sine and cosine terms of the periodic signal of ω_i angular velocity. The reference epoch is contained in the t_0 term. A sum of all above constitute a deterministic part of the time series. The ε term represents the stochastic part. It is worth noting, that the time series have to be pre-processed before Eq. (7.1) is employed. In the following research, the outliers were removed using the Interquartile Range rule (IQR), assuming values larger than 3 times the IQR value as outliers. Offsets were removed using epochs defined by the International GNSS Service (IGS), but also supported by the manual inspection. Equation (7.1) accounts only for the annual and semi-annual seasonal signatures by setting the maximum i to 2. If any other seasonal term is to be modelled, then i has to increase. Vector of time series parameters constructed as:

$$\mathbf{x} = [y_0, v_y, a_1, b_1, a_2, b_2]^T \quad (7.2)$$

is most often resolved using the simplest least-squares approach. In this case, the solution is given by:

$$\mathbf{x} = [\mathbf{A}^T \mathbf{C}_y^{-1} \mathbf{A}]^{-1} \mathbf{A}^T \mathbf{C}_y^{-1} \mathbf{y} \quad (7.3)$$

where \mathbf{A} is the design matrix for the time series model defined, \mathbf{y} is the vector with input data, while \mathbf{C}_y is the covariance matrix of noise in the observations. If the covariance matrix differs from the identity matrix, i.e. the errors of individual observations are included, the least-squares approach is changed to the Weighted Least-Squares (WLS) estimation. The uncertainties of parameters contained in \mathbf{x} are estimated using:

$$\mathbf{C}_x = [\mathbf{A}^T \mathbf{C}_y^{-1} \mathbf{A}]^{-1} \quad (7.4)$$

Then, the amplitude of the seasonal signal is computed as:

$$A = \sqrt{a^2 + b^2} \quad (7.5)$$

with its uncertainty estimated using, e.g. Rice distribution (Rice 1944).

With this approach, the determined amplitudes are time constant, which means that no variability is estimated within the vector \mathbf{x} . Basing on that, if the parameters describing the seasonal signatures were characterized by any time variability, this mismodelled effect will be transferred to the stochastic part. The construction of the covariance matrix has always been a difficulty. To keep it simple, one can put the uncertainty of the observations on the diagonal of this matrix which corresponds to white noise. However, this leads to an underestimation of the error in the estimated parameters in vector \mathbf{x} . A great alternative, which helps to account for the power-law noise, has been introduced to geodetic community in 90's in a form of Maximum Likelihood Estimation (MLE). Within this method, the preferred time series model is chosen, including the stochastic part character, basing on the values of log-likelihood function. The result is a realistic covariance matrix. It has been already implemented in the Hector (Bos et al. 2013) and CATS (Williams 2008) software and broadly used when the position time series are examined. The assumption of the white-noise-only causes that the covariance matrix of observations is constructed basing on the observation errors with no correlation between individual observations being included, as in:

$$\mathbf{C}_y = a^2 \cdot \mathbf{I} \quad (7.6)$$

where term a is the amplitude of white noise and \mathbf{I} is the identity matrix. Accounting for a power-law noise using MLE, the covariance matrix is re-constructed to a form of:

$$\mathbf{C}_y = a^2 \cdot \mathbf{I} + b_\kappa^2 \cdot \mathbf{J}_\kappa \quad (7.7)$$

where b_κ is the amplitude of the power-law noise and \mathbf{J}_κ is the power-law noise matrix. Both are estimated for a power-law noise described by spectral index κ . Now, the estimates of \mathbf{x} and \mathbf{C}_x are provided with the MLE algorithm assuming the combination of power-law and white noises.

Figure 7.1 presents the amplitudes of annual and semi-annual signals estimated with MLE, assuming their time-constancy. The estimates are provided for the IGS stations contributing to ITRF2014 (Altamimi et al. 2016) in the vertical direction. The time series were reprocessed within the second reprocessing campaign, called repro-2 (Rebischung et al. 2016). We removed outliers using 3-times-IQR criterion. The offsets were assumed using the epochs reported by IGS and supported by manual identification. Annual amplitudes range between 0.3 and 11.3 mm. The largest values were noticed for Asia and South America. Semi-annual amplitudes are few times lower than those for annual signatures, between 0.1 and 2.5 mm in the most extreme cases. Along with the deterministic model, the stochastic part character is also examined. Figure 7.2 presents three parameters of the power-law noise: spectral index, amplitude and fraction, being the percentage contribution of noise within the white plus power-law noise combination; all, combined together, allow to identify and reconstruct the noise. Spectral indices are close to -1 for the majority of stations,

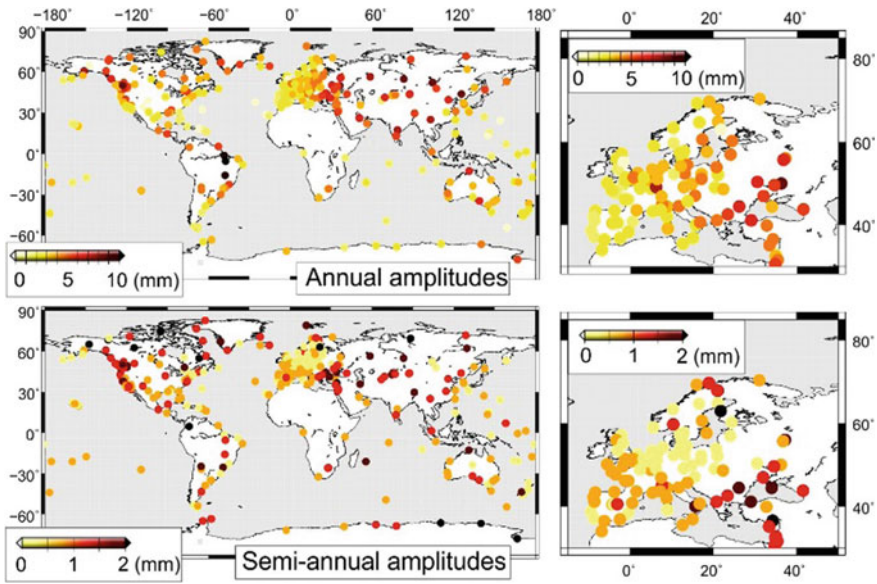


Fig. 7.1 Amplitudes of annual (top) and semi-annual (bottom) seasonal signatures constant over time and estimated with the MLE approach for a set of global (left) and European (right) ITRF2014 stations. The estimates are provided for the vertical component. The uncertainties of amplitudes, estimated assuming a combination of power-law and white noise, are not higher than 0.5 mm

indicating a flicker noise present in most observations. Amplitudes of power-law noise are much higher for the northern part of North America and Central Europe, than they are for any other part of the World. Also, a clear latitudinal dependence of the percentage contribution of power-law noise is observed. White noise outruns the power-law noise within the equatorial area, while the power-law noise dominates over white noise in higher latitudes.

7.2.2 Moving Ordinary Least-Squares (MOLS)

To provide an insight on the variability of the annual and semi-annual amplitudes over time we split the time series into segments of 3 years, each separated by 1 year. Thus, each segment overlaps the next one by 2 years. Now, the annual and semi-annual amplitudes are estimated separately for each segment with the constant-amplitude approach (previous equations) with a linear interpolation to generate a single time-varying seasonal signal. This method is named as the Moving Ordinary Least-Squares (MOLS). It is easy to implement, allows to estimate the time-varying signals, deals well with offsets and missing data.

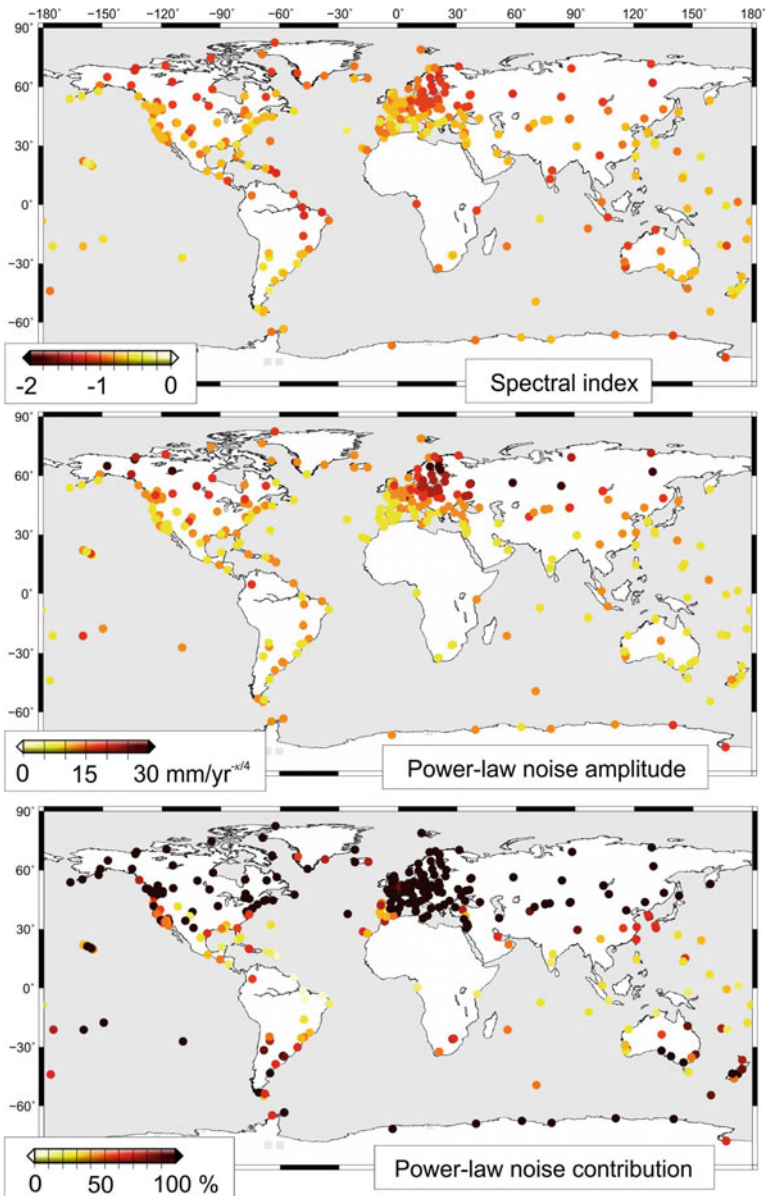


Fig. 7.2 Parameters of power-law noise characterizing the GNSS position time series; the estimates are provided with the MLE approach for a set of global ITRF2014 stations. Spectral indices (top), power-law noise amplitude (middle) and power-law noise contribution into a white plus power-law noise combination (bottom) are plotted. These three parameters allow to explicitly identify the power-law noise. Also, a power-law noise can be re-built basing on them, see further description

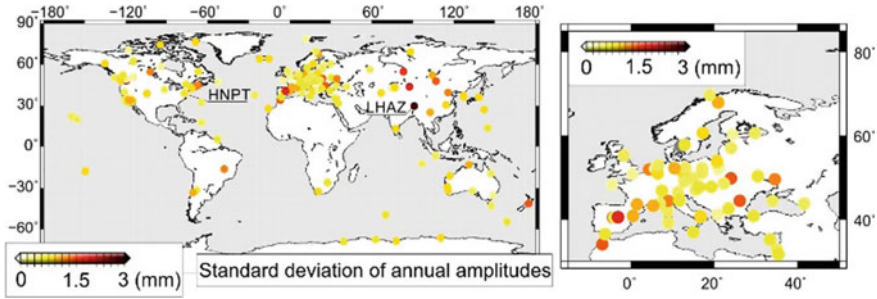


Fig. 7.3 Standard deviations (mm) of the annual amplitudes estimated with the MOLS approach for the vertical component. Two stations, for which extreme values were obtained are marked. The HNPT (USA) station is characterized by the minimum standard deviation of the annual amplitudes equal to 0.24 mm. For the LHAZ (China) station, the maximum changes of the annual curve were noticed with their standard deviation of 2.75 mm

Figure 7.3 presents the standard deviation of the annual amplitude, estimated with MOLS, for the GPS stations spanning at least 13 years. The largest variations of the annual amplitude are noticed for Asian and Eastern European stations. The greatest standard deviation of annual amplitudes equal to 2.75 mm is found for the Chinese LHAZ GPS station. For about 15% and 30% of stations, the value of standard deviation is, respectively, larger than 1.0 mm and smaller than 0.5 mm.

7.2.3 Wavelet Decomposition (WD)

Wavelet Decomposition (WD) enables to reliably capture the time-varying seasonal signatures upon the different resolution levels (Fig. 7.4). These are estimated basing on the sampling interval of data and the type of mother-wavelet employed. The seventh and eighth levels of Meyer's wavelet (Meyer 1990) are appropriate for daily observations to sufficiently capture annual and semi-annual signals by modelling all changes with periods between 128 and 512 days (Table 7.1). However, no separation between signal and noise is provided; with a use of wavelet decomposition one models all changes in the assumed frequency band, meaning both a signal and a noise.

7.2.4 Singular Spectrum Analysis (SSA)

Singular Spectrum Analysis (SSA; Broomhead and King 1986) allows to model time-varying signals basing on the Empirical Orthogonal Functions (EOFs) (Fig. 7.5). This works because the annual and semi-annual are normally above the noise level in the

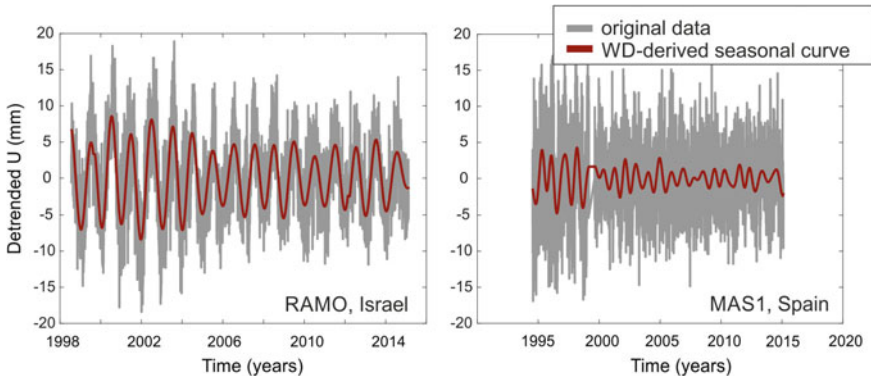


Fig. 7.4 Seasonal signatures, i.e. annual and semi-annual periods, derived by the WD for two ITRF2014 stations: RAMO (Israel) and MAS1 (Spain). Time-variability of both amplitudes may be noticed

Table 7.1 Periods determined with wavelet decomposition by various decomposition levels for daily observations. We employ details 7th and 8th to capture annual and semi-annual time-varying seasonal signals

Description	From	To
A8	1.1 years	Infinity
D8	7 months	1.4 years
D7	4 months	9 months
D6	2 months	5 months
D5	24 days	3 months
D4	12 days	37 days
D3	6 days	18 days
D2	3 days	10 days
D1	2 days	5 days

time series and well defined. As a result, these signals are part of the first set of EOFs. Note that if the noise also contains an annual or semi-annual component, this will be included in the EOFs. There is no separation of signal and noise. Its performance is strictly linked to the length of the time window employed, with the 3-year length being applied the most often. Chen et al. (2013) examined the impact that different lengths may have on the SSA-derived curves, but they did not quantify the noise which may be absorbed at the same time. Also, the absorption of noise has been mentioned lately by Xu and Yue (2015), but no specific numbers have been provided. Klos et al. (2018b) analyzed 2-, 3- and 4-year windows and proved that longer window lengths perform better for higher noise amplitudes.

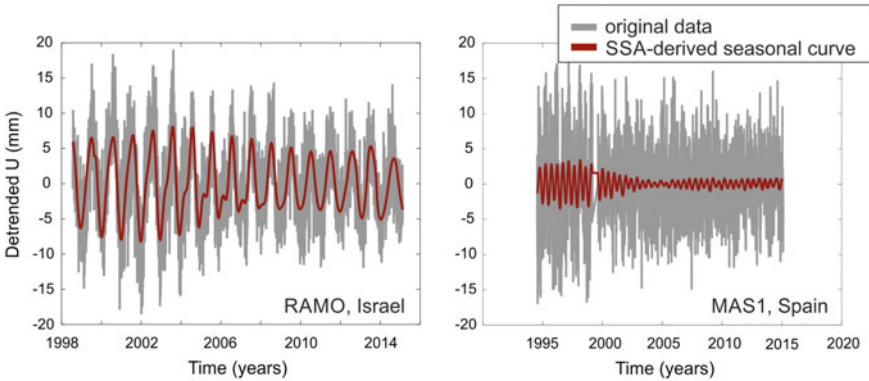


Fig. 7.5 Seasonal signatures, i.e. annual and semi-annual periods, derived by SSA for two ITRF2014 stations: RAMO (Israel) and MAS1 (Spain). Time-variability of both amplitudes may be noticed. No separation between signal and noise is provided

7.2.5 Kalman Filter (KF)

Kalman filter (KF; Kalman 1960) is employed to provide the estimates of y_0 , v_y , a_i and b_i from Eq. (7.1). However, as shown by Davis et al. (2012), the $a_i(t)$ and $b_i(t)$ are becoming now instantaneous amplitudes, consisting of a mean value and a random walk component:

$$y(t) = y_0 + v_y(t - t_0) + \sum_{i=1}^2 [a_i(t) \sin(\omega_i(t - t_0)) + b_i(t) \cos(\omega_i(t - t_0))] \quad (7.8)$$

No estimates of noise term $\varepsilon(t)$ is provided in Eq. (7.8) (compare to Eq. (7.1)), resulting in a flat power spectrum of the GPS position time series below the annual frequency. Didova et al. (2016) proved that adding the noise term in a form of third-order autoregressive process (AR(3)) to Eq. (7.8) may help to mimic a power-law noise present in the GPS position time series well. The authors showed, that a proper tuning of standard deviations of both $a_i(t)$ and $b_i(t)$ provides no power leakage between low and high frequencies. Klos et al. (2018b) assumed different values for the changes of $a_i(t)$ and $b_i(t)$ variances in the consecutive time steps. Then, they implemented both the Davis et al. (2012) and Didova et al. (2016) filters, proving that for a normal noise level of $10 \text{ mm/yr}^{0.25}$, using the former produces large misfits of even 1.15 mm between synthetic and KF-derived seasonal signature. The authors advised to use the third-order autoregressive process to mimic the power-law noise with its coefficients being estimated by its fitting to a pure flicker noise. This implementation of Kalman Filter is also used in this research (Fig. 7.6). Worth noting is the fact, that letting the $a_i(t)$ and $b_i(t)$ variances to change too much, the method-derived seasonal signal will contain also a part of the noise, leading to underestimates of trend uncertainty.

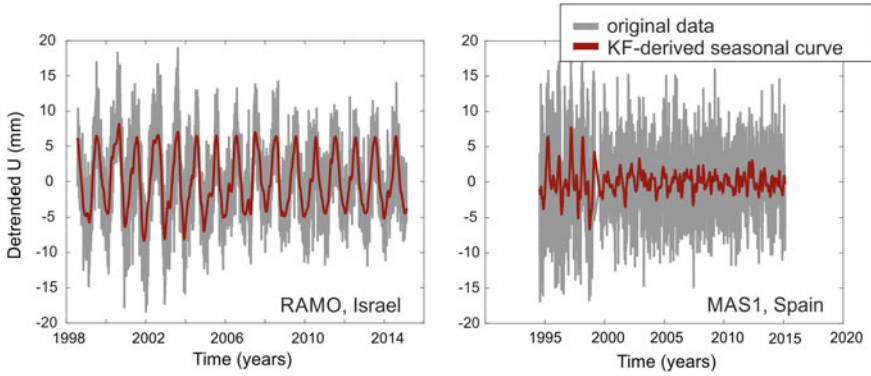


Fig. 7.6 Seasonal signatures, i.e. the annual and semi-annual periods, derived by the Kalman Filter for two ITRF2014 stations: RAMO (Israel) and MAS1 (Spain). Time-variability of both amplitudes may be noticed. A separation between seasonal signal and a noise is provided by a proper tuning of $a_i(t)$ and $b_i(t)$ (Eq. 7.8) variances and by adding a third-order autoregressive noise (AR(3)) to mimic a power-law noise present in the GPS position time series

7.2.6 Adaptive Wiener Filter (AWF)

The Adaptive Wiener Filter (AWF) has been introduced lately by Klos et al. (2018c) to model seasonal signals with the time-varying amplitudes. It is based on adapting the Wiener Filter (WF), according to the noise type and level found in the observations. In this way, the time-varying part which is greater than the assumed noise level is being found as significant and modelled. This provides a proper separation between seasonal signal and noise level.

To understand the Adaptive Wiener Filter properly, one should start from the Davis et al. (2012) filter, i.e. Eq. (7.8), and describe the seasonal signature using a time-constant s_i^{const} and a random s_i^{rand} signals:

$$\begin{aligned}
 s_i^{total} &= (a + \delta a_i) \cos(\omega_0 t_i) + (b + \delta b_i) \sin(\omega_0 t_i) \\
 &= [a \cos(\omega_0 t_i) + b \sin(\omega_0 t_i)] + [\delta a_i \cos(\omega_0 t_i) + \delta b_i \sin(\omega_0 t_i)] \\
 &= s_i^{const} + s_i^{rand}
 \end{aligned} \tag{7.9}$$

where a and b are constant values. The angular velocity of the annual signal is provided within ω_0 parameter. The random signal s_i^{rand} is characterized by the random variables δa_i and δb_i . These may be estimated using the Gaussian variables v_i and w_i of known standard deviation σ using:

$$\begin{aligned}
 \delta a_i &= \phi \cdot \delta a_{i-1} + v_i \\
 \delta b_i &= \phi \cdot \delta b_{i-1} + w_i
 \end{aligned} \tag{7.10}$$

The ϕ parameter is the first-order autoregressive coefficient (AR(1)), which should be slightly lower than 1 so as not to allow the time-varying seasonal signal to increase over time.

The time-constant part of Eq. (7.9) can be reliably estimated using WLS, and removed from the seasonal signatures. Now, the random part is estimated. Let us assume that $\delta b_i = 0$, so the estimates of the s_i^{rand} autocovariance are provided as:

$$\begin{aligned} \gamma(s_i^{rand}, s_{i+k}^{rand}) &= \text{cov}(\delta a_i \cdot \delta a_{i+k} \cos(\omega_0 t_i) \cos(\omega_0 t_{i+k})) \\ &= \text{cov}\left(\delta a_i \cdot \delta a_{i+k} \frac{1}{2} [\cos(\omega_0(t_i + t_{i+k})) + \cos(\omega_0 k)]\right) \end{aligned} \quad (7.11)$$

The AR(1) process is employed to let the seasonal signatures to vary over time is invariant. The variability of the seasonal signal s_i^{rand} is however ensured by the modulation within the cosine function. Now, the average autocovariance function is employed to estimate the one-sided spectral density function $S(\omega)$, as:

$$S(\omega) = \frac{2\sigma_v^2}{\pi} \left[\frac{1}{(1 - 2\phi \cos(\omega + \omega_0) + \phi^2)} + \frac{1}{(1 - 2\phi \cos(\omega - \omega_0) + \phi^2)} \right] \quad (7.12)$$

where $\omega = 2\pi f/f_s$ with f being the frequency and f_s the sampling frequency. So far, it was assumed that $\sigma_w = 0$. To also include the σ_w , we can easily replace σ_v^2 with $\sigma_v^2 + \sigma_w^2$.

Now, the Wiener filter is constructed using all the information provided above. Firstly, the Fourier transform $Y(\omega_i)$ of time series y_i is computed as:

$$Y(\omega_i) = F(y_i) \quad (7.13)$$

From this Fourier transform we can compute the power spectral density $S(\omega_i)$ by computing the periodogram as explained in Chap. 2. Then, we define the optimal filter $\Phi(\omega_i)$ in the frequency domain as:

$$\Phi(\omega_j) = \frac{S(\omega_j)}{S(\omega_j) + W(\omega_j)} \quad (7.14)$$

where $W(\omega_j)$ is the power spectral density of noise as function of the angular velocity. This power spectral density is employed to adapt the Wiener Filter to the noise level and type the time series are characterized by. For the pure power-law noise which characterizes the GPS position time series, the estimates of $W(\omega_j)$ are given as:

$$W(\omega_j) = \frac{\sigma_{pl}^2}{\pi} \left(2 \sin \frac{\omega_j}{2}\right)^k \approx \frac{\sigma_{pl}^2}{\pi} \omega^k \quad (7.15)$$

where κ is the spectral index of noise. The parameter σ_{pl}^2 is the standard deviation of the power-law noise, given in mm. This noise model, employed to construct the optimal filter, ensures obtaining the best separation between signal and noise. To model each individual series, the estimates of spectral indices, standard deviations of noise and its fraction delivered with MLE, should be previously performed, as shown in Fig. 7.2.

Now, the time-varying seasonal signal \hat{s} is estimated using the inverse Fourier transform:

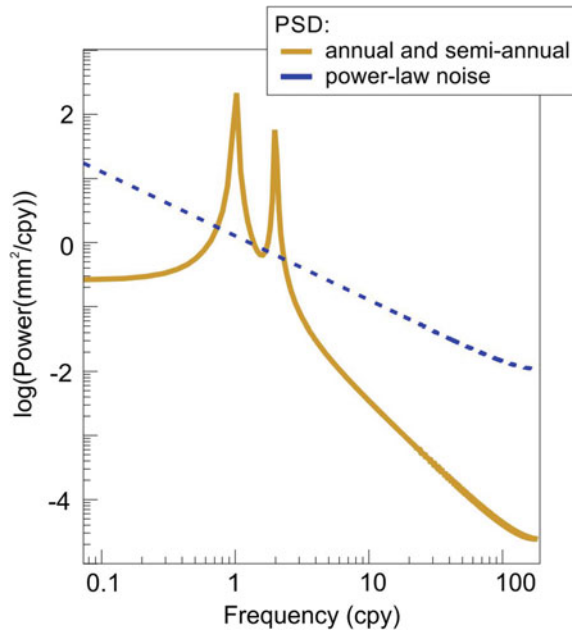
$$\hat{s}_i = F^{-1}(\Phi(\omega_i)Y(\omega_i)) \tag{7.16}$$

To obtain a total time-varying seasonal signal estimated with AWF, the estimates of varying seasonal signal computed with Eq. (7.16) should be added to the time-constant seasonal signal estimates provided by the weighted least-squares approach.

The exemplary one-sided spectral density function estimated for annual and semi-annual signatures is shown in Fig. 7.7. In addition to $S(f)$, we also provided a plot of $W(f)$, being a power spectral density of the power-law noise process. The closer ϕ is to 1, the sharper peaks of annual and semi-annual signals will be observed.

Figure 7.8 presents the AWF estimates of seasonal signals of vertical position time series for two ITRF2014 stations. A clear time-variability of seasonal amplitudes is observed for both, with a separation between signal and noise, guaranteed by the proper assumption of noise model during the construction of Wiener Filter in

Fig. 7.7 The one-sided power spectral density function of annual and semi-annual signatures $S(f)$, plotted in yellow solid line, along with the estimates of the power spectral density of the power-law noise process, $W(f)$, plotted in dashed-blue



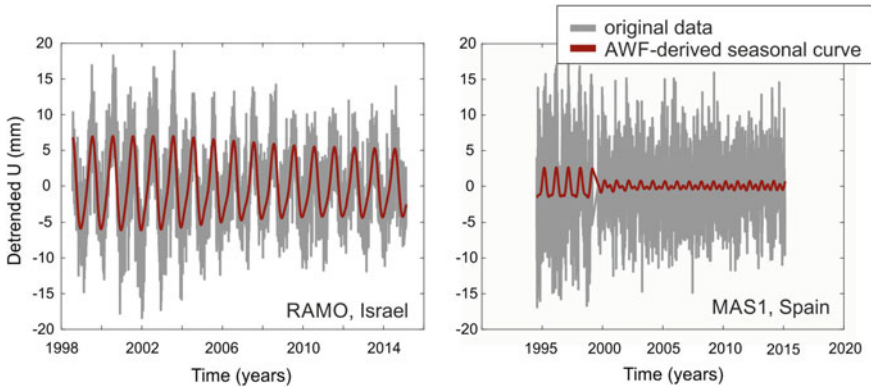


Fig. 7.8 Seasonal signatures, i.e. the annual and semi-annual periods, derived by the Adaptive Wiener Filter for two ITRF2014 stations: RAMO (Israel) and MAS1 (Spain). Time-variability of both amplitudes may be noticed. A separation between seasonal signal and a noise is provided by assuming a power spectral density of the noise model which characterizes the individual time series during the construction of the filter, see Eq. (7.14)

Eq. (7.14). It is worth noting that the noise model is being assumed and constructed separately for each individual station.

7.3 Comparison of Algorithms for the Synthetic Dataset

To mimic the GPS observations, we synthesized a number of 500 time series of a length of 16 years. A pure flicker noise was assumed with amplitudes varying between 7 and 21 mm/yr^{0.25} from series to series. This range of amplitudes covers all values met in the GPS position time series: from low to high noise levels. To the noise content, annual and semi-annual signals were added with mean amplitudes of 3 and 1 mm, respectively, and of phase lags between January and June. The annual and semi-annual amplitudes were allowed to vary over time with a standard deviation of 1 and 0.5 mm, respectively. The synthetic time series were then modelled with methods presented in the previous paragraph. Each of the curves we delivered with different methods is characterized by its ‘misfit’, meaning a standard deviation between synthetic and estimated seasonal signal (Table 7.2). The larger the misfit value, the worse is the fit of the estimated curve with respect to the synthetic seasonal. Having estimated the curves, we removed them and examined the character of residuals. All methods are being compared to the ‘no seasonal assumed’ case, which means that the seasonal signal was not modelled.

For the low noise level we synthesized, assuming no seasonal signal caused a misfit between simulated and estimated curves of 2.39 mm (Table 7.2). The WLS approach, which allows to estimate time-constant seasonal signals, produces a misfit

Table 7.2 An average misfit between synthetic and method-derived seasonal curve for a number of 500 simulations. Results are presented for low and high noise levels

Method	Misfit (mm)
Low noise level	
No seasonal assumed	2.39
WLS	0.56
MOLS	0.24
WD	0.24
KF	0.16
SSA	0.16
AWF	0.17
High noise level	
No seasonal assumed	2.44
WLS	1.11
MOLS	1.31
WD	1.53
KF	0.73
SSA	1.08
AWF	0.67

of 0.56 mm. MOLS as well as WD, both result in 0.24 mm misfit, while KF, SSA and newly introduced AWF, all produce the smaller misfit of 0.16–0.17 mm.

For the high noise level, assuming no seasonal signals results in a largest misfit of 2.44 mm. The WLS, MOLS, WD and SSA, all produce misfits larger than 1.0 mm. KF and AWF, both result in a similar misfit value lower than 0.8 mm, proving their appropriateness to model the time-varying curves.

The WLS approach, as expected, provides the worst estimates of synthetic time-varying curves for the series affected by low noise level. The performance of other algorithms is comparable. Changing the low into the high noise level, the synthetic time-varying curves cannot be separated from the noise as precisely as they are for the low noise level. In this case, WD performs the worst, followed by MOLS and WLS approaches. The best estimates of varying seasonal signatures are provided by KF, SSA and AWF.

The numbers presented in Table 7.3 prove that allowing the seasonal curve to vary over time always results in the underestimates of spectral indices and power-law noise amplitudes comparing to ‘actual’ value, which was synthesized. For high noise level, this reduction is caused by part of the noise from seasonal frequency band incorrectly absorbed in the estimates of seasonal varying curves. All methods are being compared to the ‘no seasonal assumed’ case, which means that the seasonal signal was not modelled. This causes an overestimation of spectral index and too large trend uncertainty estimates.

WLS provides comparably worse results, being unable to cover the entire seasonal peaks (Fig. 7.9), which is clearly observed for the low noise level. WD absorbs too

Table 7.3 Noise character derived with MLE for a number of 500 simulations after the seasonal curves were modelled and removed from the series. Results are presented for low and high noise levels for spectral index, amplitude and trend uncertainty, respectively. The amplitude and spectral index, which were synthesized, are shown in ‘Actual’ row. Also, the expected trend uncertainty for this noise level is given under the ‘Trend uncertainty’ label. This value is estimated using Eq. (29) of Bos et al. (2008) paper

Method	Spectral index κ	Amplitude (mm/yr ^{-$\kappa/4$)}	Trend uncertainty (mm/yr)
Low noise level			
No seasonal assumed	-1.76	3.39	0.475
WLS	-1.23	1.47	0.061
MOLS	-1.05	1.08	0.027
WD	-1.07	1.07	0.030
KF	-0.96	0.96	0.020
SSA	-0.98	0.98	0.021
AWF	-0.99	0.96	0.022
Actual	-1.00	1.00	0.022
High noise level			
No seasonal assumed	-1.07	11.18	0.294
WLS	-1.00	9.95	0.221
MOLS	-0.98	9.63	0.205
WD	-0.94	9.00	0.175
KF	-0.98	9.71	0.209
SSA	-0.96	9.35	0.191
AWF	-1.00	9.92	0.224
Actual	-1.00	10.00	0.222

much power from the seasonal frequency band for both low and high noise levels. Other methods behave in similar way – they are able to cover the time-variability with only small reduction in power. If the amplitude of the seasonal signal change over time, WLS will always provide the largest misfit between synthesized and estimated seasonal curve than any of the method presented here. Then, SSA, KF and AWF, all have excellent performance for low noise levels. For high noise levels, however, KF- and AWF-derived curves are the closest to the synthetic seasonal signatures. Although the fit of both methods is comparable, their real impact on the observations is seen through analysis of noise parameters. KF-subtracted curve causes a slight underestimation of the power-law noise amplitude and an overestimation of spectral index, while AWF-based provides the best separation between signal and noise, keeping the noise content intact.

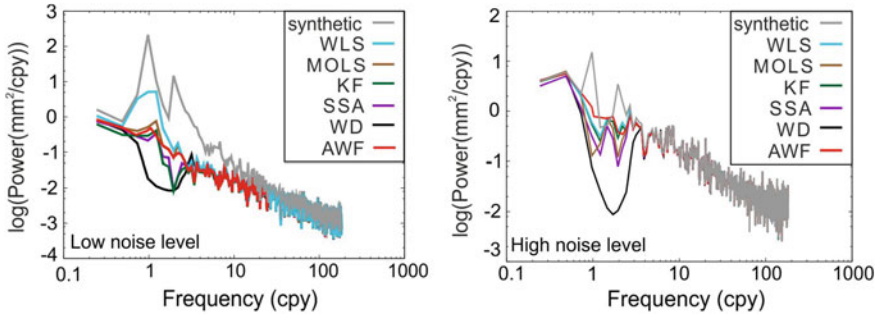


Fig. 7.9 Power Spectral Densities (PSDs) estimates provided for two noise levels synthesized within this analysis. Left: the low noise level case is shown, i.e. $1 \text{ mm/yr}^{0.25}$. Right: the high noise level is presented ($10 \text{ mm/yr}^{0.25}$). For those two noise levels, seasonal curves are estimated and removed from the series with a range of methods presented above. Then, residuals are being examined to provide the efficient assessment of noise and seasonal signal separation

7.4 Estimating the Environmental Impact

In the previous paragraphs, we presented the estimates of time-varying seasonal signatures; annual and semi-annual curves were accounted for. Though the impact the environment has on the GPS position time series is widely acknowledged at the moment, until now, we did not consider phenomena seasonal curves are caused by. We only employed methods which allow the seasonal curve to vary over time to model them in the most reliable way. Otherwise, the uncertainty of velocity might be greatly affected and misestimated.

In the following paragraph, we prove that the non-tidal atmospheric, non-tidal oceanic and continental hydrospheric loadings, all contribute significantly into the position time series (Fig. 7.10), with annual amplitudes being mostly influenced by above. The most common approach to consider the environmental impact is to directly subtract the environmental loading models from the GPS position time series for corresponding epochs. In this way, the annual amplitudes are reduced when the environmental loading models are accounted for. This approach also causes the root-mean-square value reduction (Fig. 7.11).

For this research we used Environmental Loading Models (ELM) provided by the EOST Loading Service (<http://loading.u-strasbg.fr/>). Among others, we chose ERA (ECMWF Re-Analysis) Interim (Dee et al. 2011), MERRA (Modern Era-Retrospective Analysis) land (Reichle et al. 2011) and ECCO2 (Estimation of the Circulation and Climate of the Ocean version 2) (Menemenlis et al. 2008). All loading models were decimated into daily sampling rate to correspond to position time series. For a set of the ITRF2014 vertical position time series, a mean reduction of the root-mean-square value of vertical component is larger than 20% for non-tidal atmospheric loading (ERAIN), larger than 5% for continental hydrology loading (MERRA) and almost insignificant when non-tidal ocean loading (ECCO2) is con-

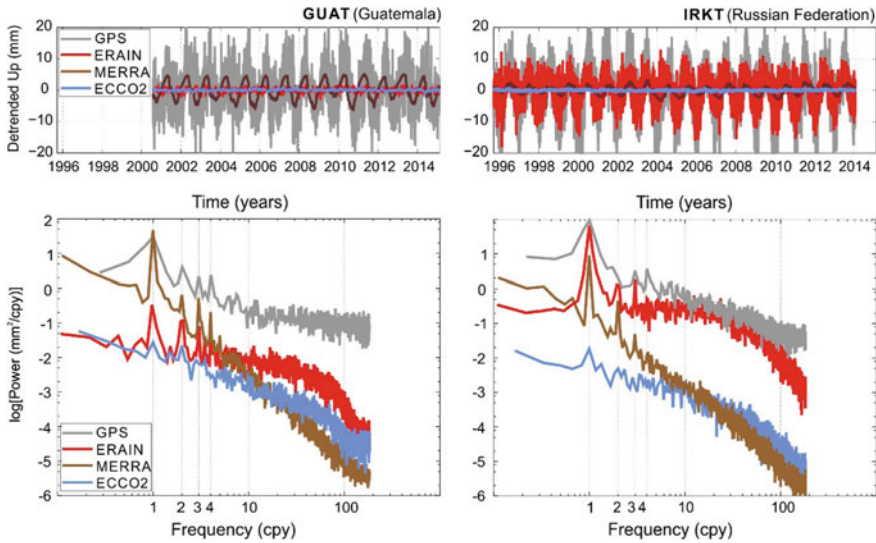
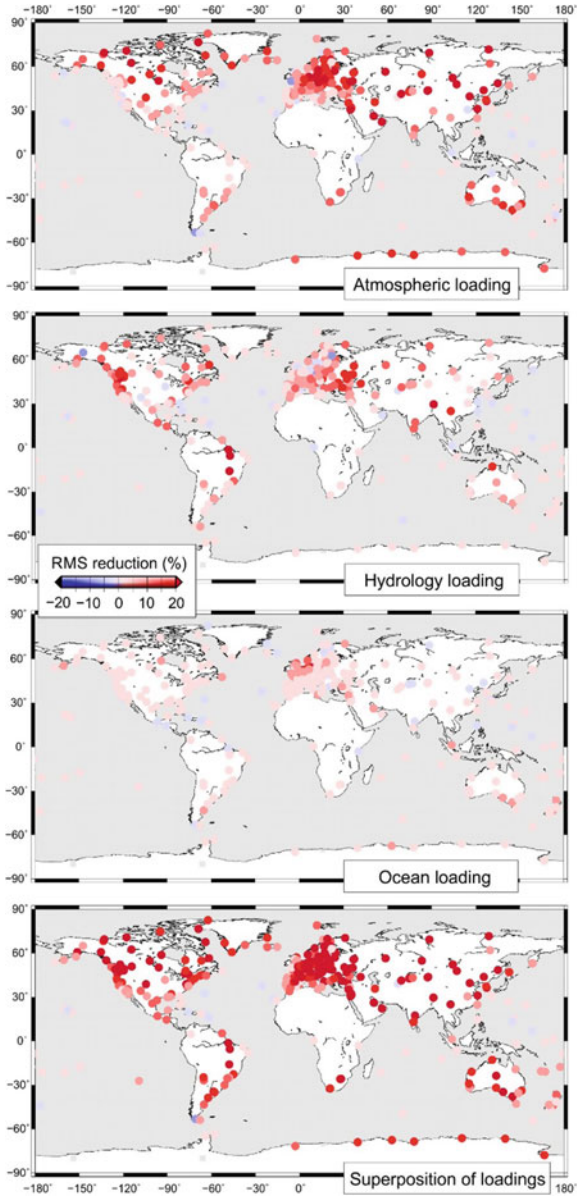


Fig. 7.10 Top: Detrended GPS vertical position time series for two ITRF2014 GNSS stations of different locations, along with Environmental Loading Models: the non-tidal oceanic (ECCO2), atmospheric (ERAIN) and continental hydrology (MERRA) loading model are plotted, respectively, in blue, red and brown. Worth noting are different root-mean-square values of loading effects, depending on the station's location. Bottom: the power spectral density estimates of the above. The annual and semi-annual curves are the most energetic ones

sidered. Atmospheric loading affects mainly Asian, European and Canadian areas, hydrospheric loading significantly contributes to position time series for east European, south Asian and Brazilian stations, while ocean loading is significant only for the Northern Sea coastal stations. Once the loading effects are summed and removed from the position time series, the mean reduction of the root-mean-square value is larger than 40% for the global set of stations, induced mostly by atmospheric loading, which contributes the most to this combination. However, as emphasized by Santamaría-Gómez and Mémin (2015), this reduction is only related to the reduction of white noise component, having nothing in common with a real impact the environmental loadings may have on the position time series.

Lately, Klos et al. (2018a) noticed that environmental loadings are characterized by various types of noises. From Fig. 7.10, we can notice that hydrospheric and oceanic loadings are characterized by power-law noise, with spectral indices slightly different from those of the position time series. Atmospheric loading, which predominates in the ELM, has autoregressive properties. Therefore, a direct removal of loading effects may cause a significant change of noise character of the GPS position time series, underestimating the velocity uncertainty at the same time if the noise model is not adapted accordingly. Wherefore, we propose a completely new approach to include the impact the environment has on the position time series. We model the superposition of environmental loadings using the SSA approach to deliver

Fig. 7.11 The root-mean-square (RMS) reduction of the GPS position time series after individual loading models are removed. The non-tidal atmospheric (ERAIN), continental hydrology (MERRA) and ocean (ECCO2) loadings are presented. The RMS reduction after subtraction of the superposition of loadings is presented at the bottom. Please note, that mass is not conserved during a simple summing of models. Reductions are presented for the ITRF2014 position time series in a vertical direction



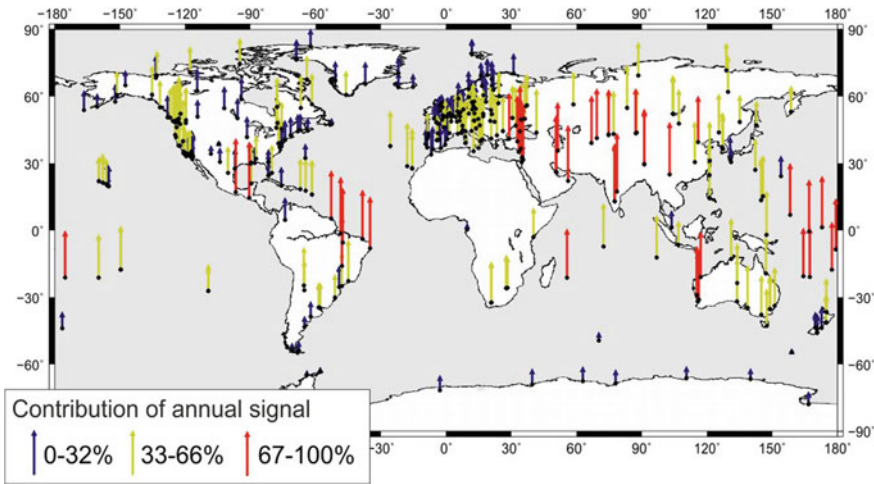


Fig. 7.12 Contribution of annual signal into the superposition of environmental loading models, presenting the total variance of signal explained by the annual signal

the time-varying seasonal changes. Due to significant changes in the standard deviation of individual loading models depending on the station’s location, the annual signal contributes differently to the entire loading signal (Fig. 7.12). The most significant amplitudes of annual signal are found for Asian, Pacific and South American stations. These are followed by eastern European and Australian and North American sites. Annual signal contributes little to the seasonal deformations of Earth’s crust in Europe, Greenland, Antarctica and Canada.

Now, this SSA-derived seasonal curve can be subtracted from the vertical position time series. In this way, the impact that the environment has on the station’s position is reduced with no influence on the noise properties (Fig. 7.13). This implies that the afore mentioned power-law plus white noise model is still an adequate noise model in the analysis of the GPS time series. Direct removal of environmental loadings causes a reduction in a position time series power for frequencies between 8 and 80 cpy. This reduction will directly affect the uncertainties of velocity, leading to their underestimation. The reason is that the reduction of power in this specific frequency band results in a too low value of the spectral index of the fitted power-law noise. Using the seasonal curve with time-varying amplitudes estimated using SSA, KF or AWF, seasonal peaks are reduced significantly, with almost no influence on power estimates. Therefore, the approach presented by Klos et al. (2018a) can be recommended to account for the environmental loading effects and remove their impact on the position time series.

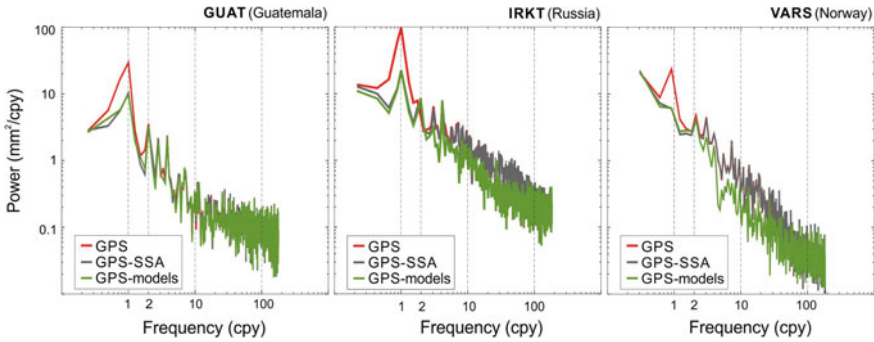


Fig. 7.13 Power spectral density estimate provided for GUAT (Guatemala), IRKT (Russia), and VARS (Norway) stations. The power of vertical GPS position time series (in red) is plotted against the residuals after loading models were subtracted directly from series (in green). The residuals were also examined after the SSA-derived seasonal-loading-curve was subtracted (in blue). An absorption in power is observed in the first case, especially for frequencies between 8 and 80 cpy. In the latter, seasonal peaks are reduced, with no significant influence on residuals

7.5 Summary

Geodetic observations are characterized by different types of noise affecting the estimates. Beyond noise, also seasonal signatures are present, which causes are not entirely recognized. Whether they arise from real geodynamic phenomena, systematic errors or numerical artefacts, they should be modelled and removed before the velocity and its uncertainty is being estimated. We deliver a comprehensive description of mathematical methods employed to model the seasonal curves within the GNSS position time series. Both time-constancy and time-changeability of amplitudes of seasonal signals are considered.

Singular Spectrum Analysis, Kalman Filter, Wavelet Decomposition and Adaptive Wiener Filter were examined basing on the synthetic time series. Primarily, it was proven that Wavelet Decomposition subtracts lots of the power from the modelled frequency band. Singular Spectrum Analysis performance is better, but its effectiveness is related to the length of the time window we use (Klos et al. 2018b). Kalman Filter gives the most appropriate estimates of seasonal curves, but only Adaptive Wiener Filter maintains the noise properties intact. The latter is provided as filter is constructed basing on the noise properties of data we examine.

Methods mentioned above provide an accurate modelling of seasonal curves on a station-by-station basis, with no research on their origin. To do so, the non-tidal atmospheric, ocean and continental hydrology loadings should be accounted for. We showed how this should be performed, so as not to influence the stochastic part of position time series. The common approach here is to directly subtract the loading models from the series. However, this causes a change in a type of noise, position time series are characterized by, especially for frequencies between 8 and 80 cpy. To remove the impact environment has on the GNSS-observed seasonal curves, an alter-

native approach should be then employed. We presented that modelling a seasonal curve directly for loading models and then removing this curve from position time series helps to account for the environmental impact, keeping the noise properties of position time series intact.

Acknowledgements We would like to thank the IGS service for providing the ITRF2014 position time series at http://itrf.ensg.ign.fr/ITRF_solutions/2014/, and the EOST service for providing the environmental loading models at <http://loading.u-strasbg.fr/>.

This research is financed by the National Science Centre, Poland. The grant was received within the SONATA-12 call, no. UMO-2016/23/D/ST10/00495. Anna Klos is supported by the Foundation for Polish Science (FNP). Machiel S. Bos was sponsored by national Portuguese funds through FCT in the scope of the Project IDL-FCT-UID/GEO/50019/2019 and Grant Number SFRH/BPD/89923/2012.

References

- Agnew D.C., Larson K.M. (2007): Finding the repeat times of the GPS constellation. *GPS Solut.*, 11(1): 71–76, <https://doi.org/10.1007/s10291-006-0038-4>.
- Altamimi Z., Rebischung P., Métivier L., Collilieux X. (2016): ITRF2014: A new release of the International Terrestrial Reference Frame modelling nonlinear station motions. *J. Geophys. Res.: Solid Earth*, 121: 6109–6131, <https://doi.org/10.1002/2016jb013098>.
- Amiri-Simkooei, A. R. (2013): On the nature of GPS draconitic year periodic pattern in multivariate position time series, *J. Geophys. Res. Solid Earth*, 118, 2500–2511, <https://doi.org/10.1002/jgrb.50199>.
- Amiri-Simkooei A.R., Mohammadloo T.H., Argus D.F. (2017): Multivariate analysis of GPS position time series of JPL second reprocessing campaign. *J. Geod.*, 91: 685–704, <https://doi.org/10.1007/s00190-016-0991-9>.
- Beavan J. (2005): Noise properties of continuous GPS data from concrete pillar geodetic monuments in New Zealand and comparison with data from U.S. deep drilled braced monuments. *J. Geophys. Res.*, 110, B08410, <https://doi.org/10.1029/2005jb003642>.
- Blewitt G., Lavallée D. (2002): Effect of annual signals on geodetic velocity. *J. Geophys. Res.*, 107, B7,2145, <https://doi.org/10.1029/2001jb000570>.
- Blewitt G., Lavallée D., Clarke P., Nurutdinov K. (2001): A new global mode of Earth deformation: seasonal cycle detected. *Science*, 294(5550): 2342–2345, <https://doi.org/10.1126/science.1065328>.
- Bogusz J., Klos A. (2016): On the significance of periodic signals in noise analysis of GPS station coordinates time series. *GPS Solut.*, 20(4): 655–664, <https://doi.org/10.1007/s10291-015-0478-9>.
- Bos M.S., Bastos L., Fernandes R.M.S. (2010): The influence of seasonal signals on the estimation of the tectonic motion in short continuous GPS time-series. *J. Geodyn.*, 49: 205–209, <https://doi.org/10.1016/j.jog.2009.10.005>.
- Bos M.S., Fernandes R.M.S., Williams S.D.P., Bastos L. (2008): Fast error analysis of continuous GPS observations. *J. Geod.* 82(3): 157–166, <https://doi.org/10.1007/s00190-007-0165-x>.
- Bos M.S., Fernandes R.M.S., Williams S.D.P., Bastos L. (2013): Fast error analysis of continuous GNSS observations with missing data. *J. Geod.*, 87: 351–360, <https://doi.org/10.1007/s00190-012-0605-0>.
- Broomhead D.S., King G.P. (1986): Extracting qualitative dynamics from experimental data. *Phys Nonlinear Phenom*, 20(2–3): 217–236, [https://doi.org/10.1016/0167-2789\(86\)90031-x](https://doi.org/10.1016/0167-2789(86)90031-x).
- Chen Q., van Dam T., Sneeuw N., Collilieux X., Weigelt M., Rebischung P. (2013): Singular spectrum analysis for modeling seasonal signals from GPS time series. *J. Geodyn.*, 72:25–35, <https://doi.org/10.1016/j.jog.2013.05.005>.

- Collilieux X., Altamimi Z., Coulot D., Ray J., Sillard P. (2007): Comparison of very long baseline interferometry, GPS, and satellite laser ranging height residuals from ITRF2005 using spectral and correlation methods. *J. Geophys. Res.*, 112, B12403, <https://doi.org/10.1029/2007jb004933>.
- Davis J.L., Wernicke B.P., Tamisiea M.E. (2012): On seasonal signals in geodetic time series. *J. Geophys. Res.*, 117, B01403, <https://doi.org/10.1029/2011jb008690>.
- Dee D.P., Uppala S. M., Simmons A. J., Berrisford P., Poli P., Kobayashi S., et al. (2011). The ERA-Interim reanalysis: configuration and performance of the data assimilation system. *Quarterly Journal of the Royal Meteorological Society*, 137, 553–597. <https://doi.org/10.1002/qj.828>.
- Didova O., Gunter B., Riva R., Klees R., Roesse-Koerner L. (2016): An approach for estimating time-variable rates from geodetic time series. *J. Geod.*, 90(11): 1207–1221, <https://doi.org/10.1007/s00190-016-0918-5>.
- Dill R., Dobszaw H. (2013): Numerical simulations of global-scale high-resolution hydrological crustal deformations. *J. Geophys. Res.: Solid Earth*, 118: 5008–5017, <https://doi.org/10.1002/jgrb.50353>.
- Dong D., Fang P., Bock Y., Cheng M.K., Miyazaki S. (2002): Anatomy of apparent seasonal variations from GPS-derived site position time series. *J. Geophys. Res.*, 107, B4, 2075, <https://doi.org/10.1029/2001jb000573>.
- Dong D., Fang P., Bock Y., Webb F., Prawirodirdjo L., Kedar S., Jamason P. (2006): Spatiotemporal filtering using principal component analysis and Karhunen-Loeve expansion approaches for regional GPS network analysis. *J. Geophys. Res.*, 111, B03405, <https://doi.org/10.1029/2005jb003806>.
- Graham S.E., Loveless, J.P., Meade B.J. (2018): Global plate motions and earthquake cycle effects. *Geochem. Geophys. Geosyst.* 19: 2032–2048, <https://doi.org/10.1029/2017gc007391>.
- Gruszczynska M., Klos A., Gruszczynski M., Bogusz J. (2016): Investigation of time-changeable seasonal components in GPS height time series: a case study for central Europe. *Acta Geodyn. Geomater.*, 13(3): 281–289, <https://doi.org/10.13168/agg.2016.0010>.
- Gruszczynski M., Klos A., Bogusz J. (2018): A filtering of incomplete GNSS position time series with probabilistic Principal Component Analysis. *Pure Appl. Geophys.*, 175: 1841–1867, <https://doi.org/10.1007/s00024-018-1856-3>.
- Kalman R.E. (1960): A new approach to linear filtering and prediction problems. *J Basic Eng-Trans ASME* 82: 35–45, <https://doi.org/10.1115/1.3662552>.
- Karegar M.A., Dixon T.H., Malservisi R., Kusche J., Engelhart S.E. (2017): Nuisance flooding and relative sea-level rise: the importance of present-day land motion. *Scientific Reports*, 7:11197, <https://doi.org/10.1038/s41598-017-11544-y>.
- King M.A., Bevis M., Wilson T., Johns B., Blume F. (2012): Monument-antenna effects on GPS coordinate time series with application to vertical rates in Antarctica. *J. Geod.*, 86(1): 53–63, <https://doi.org/10.1007/s00190-011-0491-x>.
- King, M.A., Santamaría-Gómez A. (2016): Ongoing deformation of Antarctica following recent Great Earthquakes, *Geophys. Res. Lett.*, 43, <https://doi.org/10.1002/2016gl067773>.
- King M.A., Watson C.S., Penna N.T., Clarke P.J. (2008): Subdaily signals in GPS observations and their effect at semiannual and annual periods. *Geophys. Res. Lett.*, 35, L03302, <https://doi.org/10.1029/2007gl032252>.
- Klos A., Bogusz J. (2017): An evaluation of velocity estimates with a correlated noise: case study of IGS ITRF2014 European stations. *Acta Geodynamica et Geomaterialia*, Vol. 14, No. 3 (187), 255–265, 2017. <https://doi.org/10.13168/agg.2017.0009>.
- Klos A., Bogusz J., Figurski M., Kosek W. (2015): Noise analysis of continuous GPS time series of selected EPN stations to investigate variations in stability of monument types. *Springer IAG Symposium Series volume 142, proceedings of the VIII Hotine Marussi Symposium*, pp. 19–26, https://doi.org/10.1007/1345_2015_62.
- Klos A., Bogusz J., Figurski M., Gruszczynski M. (2016): Error analysis for European IGS stations. *Stud. Geophys., Geod.*, 60(1): 17–34, <https://doi.org/10.1007/s11200-015-0828-7>.

- Klos A., Gruszczynska M., Bos M.S., Boy J.-P., Bogusz J. (2018a): Estimates of vertical velocity errors for IGS ITRF2014 stations by applying the improved Singular Spectrum Analysis Method and environmental loading models. *Pure Appl. Geophys.*, 175: 1823–1840, <https://doi.org/10.1007/s00024-017-1494-1>.
- Klos A., Bos M.S., Bogusz J. (2018b): Detecting time-varying seasonal signal in GPS position time series with different noise levels. *GPS Solut.*, 22:21, <https://doi.org/10.1007/s10291-017-0686-6>.
- Klos A., Bos M.S., Fernandes R.M.S., Bogusz J. (2018c): Noise dependent adaption of the Wiener Filter for the GPS position time series. *Math. Geosci.*, <https://doi.org/10.1007/s11004-018-9760-z>.
- Klos A., Olivares G., Teferle F.N., Hunegnaw A., Bogusz J. (2018d): On the combined effect of periodic signals and colored noise on velocity uncertainties. *GPS Solut.*, 22:1, <https://doi.org/10.1007/s10291-017-0674-x>.
- Langbein J. (2012): Estimating rate uncertainty with maximum likelihood: differences between power-law and flicker-random-walk models. *J. Geod.*, 86: 775–783, <https://doi.org/10.1007/s00190-012-0556-5>.
- Langbein J., Johnson H. (1997): Correlated errors in geodetic time series: Implications for time-dependent deformation. *J. Geophys. Res.*, 102, B1, 591–603, <https://doi.org/10.1029/96jb02945>.
- Mao A., Harrison Ch.G.A., Dixon T.H. (1999): Noise in GPS coordinate time series. *J. Geophys. Res.*, 104, B2, 2797–2816, <https://doi.org/10.1029/1998jb900033>.
- Menemenlis D., Campin J., Heimbach P., Hill C., Lee T., Nguyen A., et al. (2008): ECCO2: High resolution global ocean and sea ice data synthesis. *Mercator Ocean Quarterly Newsletter*, 31, 13–21.
- Meyer Y. (1990): *Ondelettes et Opérateurs*, vol I–III, Hermann, Paris, 1990.
- Montillet J.-P., Melbourne T.I., Szeliga W.M. (2018): GPS vertical land motion corrections to sea-level rise estimates in the Pacific Northwest. *J. Geophys. Res.: Oceans*, 123: 1196–1212, <https://doi.org/10.1002/2017jc013257>.
- Penna N.T., Stewart M.P. (2003): Aliased tidal signatures in continuous GPS height time series. *Geophys. Res. Lett.*, 30, 2184, <https://doi.org/10.1029/2003GL018828>.
- Petrov L., Boy J.-P. (2004): Study of the atmospheric pressure loading signal in very long baseline interferometry observations. *J. Geophys. Res.*, 109, B03405, <https://doi.org/10.1029/2003jb002500>.
- Reibischung P., Altamimi Z., Ray J., Garayt, B. (2016): The IGS contribution to ITRF2014. *J. Geod.*, 90: 611–630, <https://doi.org/10.1007/s00190-016-0897-6>.
- Reichle R. H., Koster, R. D., De Lannoy G. J. M., Forman B. A., Liu Q., Mahanama S. P. P., et al. (2011): Assessment and enhancement of MERRA land surface hydrology estimates. *J. Clim.*, 24, 6322–6338. <https://doi.org/10.1175/jcli-d-10-05033.1>.
- Rice S.O. (1944): Mathematical Analysis of Random Noise. *Bell Systems Tech. J.*, 23(3): 282–332, <https://doi.org/10.1002/j.1538-7305.1944.tb00874.x>.
- Santamaría-Gómez A., Bouin M.-N., Collilieux X., Wöppelmann G. (2011): Correlated errors in GPS position time series: Implications for velocity estimates. *J. Geophys. Res.*, 116, B01405, <https://doi.org/10.1029/2010jb007701>.
- Santamaría-Gómez A., Mémin A. (2015): Geodetic secular velocity errors due to interannual surface loading deformation. *Geophys. J. Int.*, 202: 763–767, <https://doi.org/10.1093/gji/ggv190>.
- Tregoning P., Watson C., Ramillien G., McQueen H., Zhang J. (2009): Detecting hydrologic deformation using GRACE and GPS. *Geophys. Res. Lett.*, 36, L15401, <https://doi.org/10.1029/2009gl038718>.
- van Dam T., Collilieux X., Wuite J., Altamimi Z., Ray J. (2012): Nontidal ocean loading: amplitudes and potential effects in GPS height time series. *J. Geod.*, 86(11): 1043–1057, <https://doi.org/10.1007/s00190-012-0564-5>.
- van Dam T.M., Wahr J., Chao Y., Leuliette E. (1997): Predictions of crustal deformation and of geoid and sea-level variability caused by oceanic and atmospheric loading. *Geophys. J. Int.*, 129: 507–517.

- van Dam T., Wahr J., Milly P.C.D., Shmakin A.B., Blewitt G., Lavallée D., Larson K.M. (2001): Crustal displacements due to continental water loading. *Geophys. Res. Lett.*, 28(4): 651–654, 2000GL012120.
- Wang W., Zhao B., Wang Q., Yang S. (2012): Noise analysis of continuous GPS coordinate time series from CMONOC. *Adv. Space Res.*, 49: 943–956, <https://doi.org/10.1016/j.asr.2011.11.032>.
- Williams S.D.P. (2003a): Offsets in Global Positioning System time series. *J. Geophys. Res.*, 108, B6, 2310, <https://doi.org/10.1029/2002jb002156>.
- Williams S.D.P. (2003b): The effect of coloured noise on the uncertainties of rates estimated from geodetic time series. *J. Geod.*, 76: 483–494, <https://doi.org/10.1007/s00190-002-0283-4>.
- Williams S.D.P. (2008): CATS: GPS coordinate time series analysis software. *GPS Solut.*, 12: 147–153, <https://doi.org/10.1007/s10291-007-0086-4>.
- Williams S.D.P., Bock Y., Fang P., Jamason P., Nikolaidis R.M., Prawirodirdjo L., Miller M., Johnson D. (2004): Error analysis of continuous GPS position time series. *J. Geophys. Res.*, 109, B03412, <https://doi.org/10.1029/2003jb002741>.
- Williams S.D.P., Penna N.T. (2011): Non-tidal ocean loading effects on geodetic GPS heights. *Geophys. Res. Lett.*, 38, L09314, <https://doi.org/10.1029/2011gl046940>.
- Xu C., Yue D. (2015): Monte Carlo SSA to detect time-variable seasonal oscillations from GPS-derived site position time series. *Tectonophys.*, 665:118–126, <https://doi.org/10.1016/j.tecto.2015.09.029>.
- Yan H., Chen W., Zhu Y., Zhang W., Zhong M. (2009): Contributions of thermal expansion of monuments and nearby bedrock to observed GPS height changes. *Geophys. Res. Lett.*, 36, L13301, <https://doi.org/10.1029/2009gl038152>.



Anna Klos received a Ph.D. degree in 2016. In 2019, she was granted with habilitation. She is currently working at the Military University of Technology (Warsaw, Poland) as associate professor. Her main research area is related to time series analysis, in terms of Earth's deformations, loading effects, tropospheric delay and their applications. She is focused on the geodetic deliverables which may be helpful for climate change studies.



Janusz Bogusz is a Professor of Geodesy at the Military University of Technology (Warsaw, Poland). His research focuses on the areas of physical geodesy, geodynamics as well as geodetic time series analysis. He is currently the chair of the Sub-Commission 3.1 “Earth Tides and Geodynamics” of the International Association of Geodesy (IAG) and a member of the Global Geodetic Observing System (GGOS) Science Panel. He is a Fellow of the IAG.



Machiel S. Bos obtained in 1996 his M.Sc. from the Delft University of Technology. In 2001, he received his Ph.D. from the University of Liverpool. Afterward, he held various post-doc positions in Sweden, the Netherlands, and Portugal. Currently, he is a post-doc at Instituto Dom Luiz. His scientific interests include ocean tide loading, GPS time series analysis, and geoid computations.



Marta Gruszczynska obtained her Ph.D. in Geodesy and Cartography from Military University of Technology (Warsaw, Poland) in 2018. During her Ph.D. studies, she dealt with GNSS data analysis and multivariate data statistics. She is currently R&D Project Manager at one of the polish space sector companies, where her activities are focused on development of innovative GNSS signals monitoring system for critical infrastructure.